

Estimating habitat extent and carbon loss from an eroded Northern blanket bog using UAV derived imagery and topography.

Journal:	<i>Progress in Physical Geography</i>
Manuscript ID	PPG-17-088.R3
Manuscript Type:	Main Article
Keywords:	Peatlands, Unmanned Aerial Vehicle, Structure from Motion, Habitat, Blanket Bog, Random Forest
Abstract:	<p>Peatlands are important reserves of terrestrial carbon and biodiversity, and given that many peatlands across the UK and Europe exist in a degraded state, their conservation is a major area of concern, and a focus of considerable research. Aerial surveys are valuable tools for habitat mapping and conservation and provide useful insights into their condition. We investigate how Structure from Motion (SfM) photogrammetry derived topography and habitat classes may be used to derive an estimate of carbon loss from erosion features in a remote blanket bog habitat. An autonomous, unmanned, aerial, fixed wing remote sensing platform (Quest UAV 300™), collected imagery over Moor House – Upper Teesdale National Nature Reserve, a site with a high degree of peatland erosion. The images were used to generate point clouds into orthomosaics and digital surface models using SfM photogrammetry techniques, georeferenced, and subsequently used to classify vegetation and peatland features. A classification of peatbog feature types was developed using a random forest classification model trained on field survey data and applied to UAV-captured products including the orthomosaic, digital surface model and derived surfaces such as topographic index, slope and aspect maps. Using the area classified as eroded peat, and the derived digital surface model, we estimated a loss of 438 tonnes of carbon from a single gully. The UAV system was relatively straightforward to deploy in such a remote and unimproved area. SfM photogrammetry, imagery and random forest modelling obtained classification accuracies of between 42% and 100%, and was able to discern between bare peat, saturated bog and sphagnum, habitats. This paper shows what can be achieved with a low-cost UAV equipped with consumer grade camera equipment, and relatively straightforward ground control, and demonstrates their potential for the carbon and peatland conservation research community.</p>

1 **Abstract**

2 Peatlands are important reserves of terrestrial carbon and biodiversity, and given that many
3 peatlands across the UK and Europe exist in a degraded state, their conservation is a major area
4 of concern, and a focus of considerable research. Aerial surveys are valuable tools for habitat
5 mapping and conservation and provide useful insights into their condition. We investigate how
6 Structure from Motion (SfM) photogrammetry derived topography and habitat classes may be
7 used to derive an estimate of carbon loss from erosion features in a remote blanket bog habitat.
8 An autonomous, unmanned, aerial, fixed wing remote sensing platform (Quest UAV 300™),
9 collected imagery over Moor House – Upper Teesdale National Nature Reserve, a site with a
10 high degree of peatland erosion. The images were used to generate point clouds into
11 orthomosaics and digital surface models using SfM photogrammetry techniques, georeferenced,
12 and subsequently used to classify vegetation and peatland features. A classification of peatbog
13 feature types was developed using a random forest classification model trained on field survey
14 data and applied to UAV-captured products including the orthomosaic, digital surface model and
15 derived surfaces such as topographic index, slope and aspect maps. Using the area classified as
16 eroded peat, and the derived digital surface model, we estimated a loss of 438 tonnes of carbon
17 from a single gully. The UAV system was relatively straightforward to deploy in such a remote
18 and unimproved area. SfM photogrammetry, imagery and random forest modelling obtained
19 classification accuracies of between 42% and 100%, and was able to discern between bare peat,
20 saturated bog and sphagnum, habitats. This paper shows what can be achieved with a low-cost
21 UAV equipped with consumer grade camera equipment, and relatively straightforward ground
22 control, and demonstrates their potential for the carbon and peatland conservation research
23 community.

25 Introduction

26 Blanket bogs are tree-less habitats that form in cool, wet, oceanic climates dominated by vascular
27 plants such as *Eriophorum* and *Calluna* spp and cushion forming bryophytes such as *Sphagnum*
28 spp. They cover roughly 4,000,000 km² land and have been estimated to store 500-600
29 gigatonnes of carbon (Yu, 2012, Holden, 2005). Because of this enormous carbon (C) stock,
30 peatland C represents an important reservoir within the global C cycle (Freeman et al. 2001).
31 Over 80% of UK peatlands are in a degraded state due mainly to past drainage, fire and grazing
32 (Joosten et al., 2012). It has been estimated that 16% of the global peatland reserve has been
33 degraded and lost owing to human activities (Littlewood, 2010). Recently, the increased
34 awareness of this global decline has resulted in a range of directives and guidelines, and in the
35 UK conservation management aimed at restoring peatlands has been implemented under the EU
36 habitats directive (Evans et al. 2014). From an ecological perspective, peatlands also represent an
37 important habitat for a number of rare and endangered plant and animal species.

38 The monitoring of blanket bogs is particularly challenging, as a consequence of their remoteness
39 and physical complexity, but a number of methods have been developed (Mc Morrow et al.,
40 2004, Evans and Lindsay, 2010, Glendell et al., 2017). Remote sensing techniques using
41 commercial satellite data are well established, and offer data at sub-10 m resolution. To date the
42 high cost of these data, and limitations due to cloud coverage or view angles, have limited the
43 value of Earth Observation (EO)-based data for this type of surveillance. Recently however, new
44 methods for capturing high resolution scenes of remote peatlands have emerged.

45 Unmanned aerial vehicles (UAVs) now offer the ecologist a useful platform for capturing images
46 of peatlands closer to the ground, i.e. below normal cloud levels. The data can be accessed
47 immediately, and ground truthing field surveys can be timed to coincide precisely with the time

1
2
3 48 of flights. UAVs allow the collection of higher resolution imagery at a lower cost than manned
4
5 49 aircraft or commercial satellite-data. UAV imagery resolution is typically less than 5cm per
6
7 50 pixel, whereas manned aircraft resolution is typically 25-12.5 cm per pixel and satellite
8
9 51 resolution is at best around 50 cm per pixel (Toth and Jozkow, 2016). Imagery acquired by the
10
11 52 older generation of satellite sensors, at around 30 m per pixel, may pick up the dominant habitat
12
13 53 but tend to lack the resolution required to represent the complex mosaics characteristic of many
14
15 54 natural and semi-natural habitats (Boyle et al, 2014).

16
17 55 Image mosaic preparation, i.e. stitching the imagery together using off the shelf tools, remains a
18
19 56 challenge due to the heterogeneity of habitats within landscape imagery, but is now automated in
20
21 57 many software packages, and orthomosaics can be readily obtained. An important recent
22
23 58 breakthrough is that a high resolution digital surface model (DSM) may also be obtained through
24
25 59 Structure from Motion (SfM) photogrammetry processing in such software, since information on
26
27 60 surface structure derived from the DSM may inform the relationship between subsequent
28
29 61 classifications and peatland condition (Anderson et al. 2010). The combination of spectral data,
30
31 62 DSM and classification techniques already available in the remote sensing scientist's toolbox
32
33 63 (Random Forest Classification, maximum likelihood etc.) now provide huge potential to develop
34
35 64 and calibrate an effective UAV-imagery based tool for peatland monitoring. Spectral and
36
37 65 textural information have been combined successfully using Random Forest (a method based on
38
39 66 machine learning that uses ensembles of decision trees to assign classes - see Breiman (2001)
40
41 67 and Gislason et al. (2006)) for predicting forest condition (Dye et al. 2012), and for looking at
42
43 68 fine scale coastal structures (Juel et al. 2015). Whilst uncertainties certainly exist in the use of
44
45 69 SfM, uncertainties are simultaneously reduced if one considers how little detailed surface
46
47
48
49
50
51
52
53
54
55
56
57
58
59
60

70 topographic information exists for remote gully environments such as at Moor House NNR, used
71 in this study.

72 In this paper we explore the potential of high spatial resolution (4 cm) true-colour (RGB)
73 imagery obtained from a UAV platform for mapping and ecologically classifying a remote
74 upland blanket bog in northern England. Since the surface topography of northern blanket bog
75 habitats determine the presence of *Sphagnum*, *Eriophorum* or *Calluna* habitats, the models
76 presented here incorporate a compound topographic index (CTI). Specifically we compared two
77 input data scenarios and quantified the difference in the resulting classification:

78 Scenario 1: True-Colour orthomosaic only

79 Scenario 2: True-Colour orthomosaic, plus slope, CTI and aspect

80 We used two scenarios so that the effect that texture information might have on the accuracy of
81 the peatland classification could be investigated. In particular we aimed to investigate the
82 capability of the imagery to define small patches (< 1m width) of the fine scale habitats such as
83 *Sphagnum* (a positive indicator of high water table), or exposed peat (negative indicator) that are
84 poorly mapped by coarser resolution EO data. We considered how the information content of the
85 input data could be maximised to improve classification accuracy. Finally we provide an
86 estimate of carbon loss from an area of eroded peat based on: the elevation model, the classified
87 eroded peat area, and the carbon density measurements taken through surveys at the site.

88 Methodology

89 Description of the study site

90 The UK Environmental Change Network (ECN) site, Moor House, Upper Teesdale, (OS Grid
91 reference NY75303331), in the North Pennine uplands (Figure 1), is England's highest and

1
2
3 92 largest terrestrial National Nature Reserve (NNR). It is a UNESCO Biosphere Reserve and a
4
5 93 European Special Protection Area. Habitats include exposed summits, extensive blanket
6
7 94 peatlands, upland grasslands and pastures grazed mainly by sheep, hay meadows and deciduous
8
9 95 woodland. A large part of the catchment of the River Tees, from its source near Great Dun Fell
10
11 96 to High Force waterfall, is included in the reserve. The site comprises two areas divided by Cow
12
13 97 Green Reservoir. The Moor House area extends from the upper edge of enclosed land in the
14
15 98 Eden Valley, over Great Dun Fell (848 m), Little Dun Fell and Knock Fell to the upper end of
16
17 99 Cow Green Reservoir on the River Tees. The gently sloping eastern side of the area is overlain
18
19 100 by poorly-drained glacial till, which has led to the development of blanket bog with peat 2-3 m
20
21 101 deep. The vegetation is dominated by *Eriophorum* spp., *Calluna vulgaris* and *Sphagnum* spp.
22
23 102 with patches of eroded blanket bog without vegetation cover. The western side is steeper and the
24
25 103 soils and vegetation are more variable. The area includes unique communities of arctic-alpine
26
27 104 plants and upland flora and fauna of conservation interest.
28
29
30
31
32
33

34 105 **Field Data Collection**

35
36 106 A vegetation and landform survey was carried out between June and September 2008, and May
37
38 107 and July 2009, as part of a wider objective to update habitat mapping within the Troutbeck
39
40 108 catchment, a small catchment within the Moor House area (Rose et al., 2016). Quadrat sampling
41
42 109 points were located systematically at the mid-points of a 100 m grid using ArcGIS (ESRI)
43
44 110 (Figure 1), and located in the field using a handheld GPS unit (Garmin eTrex Vista HCx,
45
46 111 accuracy < 3m).
47
48
49

50
51 112 Data were entered into a GIS database in the field using a modified version of the 'CS Surveyor'
52
53 113 digital data capture system designed for Countryside Survey 2007 (Maskell et al. 2008). A 2 x 2
54
55 114 m² quadrat was placed at each plot, with the diagonal orientated north-south. Within each
56
57
58
59
60

1
2
3 115 quadrat, percentage cover of all vascular plant species, and a restricted list of bryophytes, was
4
5 116 determined using visual estimation according to the technique described in Maskell et al. (2008).
6
7

8 117 **Airborne Data Collection**

9
10 118 The airborne campaigns were conducted in summer 2015 using an unmanned aerial vehicle
11
12 119 (UAV) operated by the NERC Centre for Ecology and Hydrology. The UAV, a QuestUAV
13
14 120 300™, carried a Panasonic Lumix DMC-LX7 with a 3648 x 2736 pixel detector that captured
15
16 121 JPEG images at f/1.4 and 1/2500s with an angular field of view of 73.7×53.1, providing ~4.5cm
17
18 122 pixel⁻¹ resolution at 122 m above ground level (AGL). The UAV was a 2 m wingspan fixed-wing
19
20 123 platform with up to 1 h endurance at 3 kg take-off weight and 63 km/h ground speed. The UAV
21
22 124 platform followed four flight plans over a 2400 m² area, which had been designed to ensure
23
24 125 sharp imagery was obtained at high resolution, which had large across- and along-track
25
26 126 overlapping. The UAV took 20 minutes to complete each flight plan at 122 m AGL. It was flown
27
28 127 by two trained operators and controlled by an autopilot for fully autonomous flying (Skycircuits
29
30 128 SC2, Southampton, UK). The autopilot had a dual CPU controlling an integrated attitude heading
31
32 129 reference system (AHRS) with a comprehensive onboard sensor suite (3-axis accelerometers, 3-
33
34 130 axis gyroscopes, 3-axis magnetometers, dynamic and static pressure sensors). The ground control
35
36 131 station and the UAV were radio linked, transmitting position, altitude, and status data at 2.4 GHz.
37
38 132 The weather on the date of the flights was clear and free of cloud. Flights were conducted
39
40 133 between 10:00 and 16:00 to minimise effects of shadow. Wind speeds remained below 15 knots
41
42 134 on all flights. The integrated onboard GPS updated at between 4 and 10 Hz and had a positional
43
44 135 accuracy of +/-3 m.
45
46
47
48
49
50
51

52 136

53 137 **Airborne Data Processing**

1
2
3 138 The imagery was synchronized using the GPS position and the triggering time recorded on the
4
5 139 flight logger for each image, and these were then used for the generation of an orthomosaic and
6
7 140 digital surface model (DSM). Flight altitude data were also logged and images were geotagged
8
9
10 141 with xyz coordinates for use by the image processing software. Image processing of the image
11
12 142 collection was performed in Agisoft PhotoScan Professional v1.4.2 (© 2018 Agisoft LLC, 27
13
14 143 Gzhatskaya st., St. Petersburg, Russia). Details of the steps taken in acquisition, processing and
15
16 144 modelling are shown in Figure 2. The software initially aligned the camera positions based on
17
18 145 the GPS coordinates from the flight log. Ground control points were added based on known
19
20 146 locations of static features located using 25cm Next Perspectives Aerial Photography RGB
21
22 147 Product (Infoterra Ltd). Height values were based on values obtained from the Environment
23
24 148 Agency LIDAR digital surface model which covered parts of the study area. Then a 3D point
25
26 149 cloud, and 3D mesh representing the land surface was generated at a density of 160 points m⁻²,
27
28 150 this mesh was then used for orthomosaic and DSM generation at 0.04 m resolution. The Z error
29
30 151 was computed by deducting check points Z values from the DSM value at the same point. The
31
32 152 image processing settings and associated calculated accuracies are shown in Tables 4 and 5.
33
34 153 During the stages of processing checks were made on image quality, tie point quality.

154 **Topographic Processing**

155 The DSM obtained from the image processing software was processed in ArcGIS 10.6 (ESRI,
156 2018). Slope, aspect, and a compound topographic index (CTI) (Sorensen et al., 2006) were
157 generated at 4 cm resolution (see Figure 3) to be compatible with the RGB data. These figures
158 show a subset of the data, and the gully features used for the Carbon loss estimation.
159 These data were then combined to yield a 6 band raster image containing red, green, blue, slope,
160 aspect, and CTI values at 4 cm resolution.

161

162 Image Classification

163 The classification was trained on the 8 aggregate cover classes (Table 1) using all pixels within
164 the digitised areas around each point. Specifically we compared two input data scenarios and
165 quantified the difference in the resulting classification:

166 Scenario 1: Image Classification using Original RGB bands

167 The image obtained from the SfM procedures in Photoscan was processed using only the red,
168 green and blue colourspace.

169 Scenario 2: Image Classification using Surface features and Original RGB Bands

170 The final image was processed using the red, green and blue colourspace, together with surface
171 characteristics (gullies, edges) derived from the digital surface. The additional surface
172 characteristics were added as separate bands to the image. These were slope, aspect, and CTI, all
173 generated from the surface model at 4 cm resolution in ArcGIS 10.6 (ESRI, 2017).

174 The Random Forest (RF) classifier is an ensemble method that combines CART (Classification
175 And Regression Trees) with bootstrap aggregating techniques (Breiman et al., 1984). Random
176 Forests grow a number of binary classification trees by selecting a random sample with
177 replacement from the training set (bootstrap aggregating or bagging) for each tree (Breiman,
178 1996). The predicted class for observations in the training set is the most frequent class in the
179 trees for which the observation is a member. This process is described as “voting” (Breiman et
180 al., 1984). The RF algorithm outputs the class label that received the majority of votes, and a
181 probability estimate is derived for each pixel based upon the percentage of votes. The 6 band
182 raster image, and companion training data for the 8 classes (Table 4) were supplied as inputs to

183 the algorithm, and the algorithm was processed in R (R Core Team 2015) using the Random
184 Forest package by Liaw and M. Wiener (2002), and Horning (2013)

185 **Field data Processing: Training data**

186 The plant species cover data from the quadrats were automatically assigned to the nearest
187 National Vegetation Classification (NVC), (Rodwell, 1995.) sub-community using the MAVIS
188 program (Smart, 2000) which uses Czekanowski's quantitative index of similarity, taking into
189 account the abundance as well as presence of species (Magurran, 1998). This supervised
190 classification of the data was then visually checked against photographs taken at the date of
191 sampling. If there were discrepancies the assigned class was corrected according to a visual
192 interpretation from the photography. The areas were manually digitised in GIS in order to
193 encapsulate the habitats of a similar type around the plot, so that for a 10 m diameter zone
194 around each plot, the dominant habitat type was described, and the other habitat areas removed,
195 leaving just the habitat of interest for each plot. For example *Sphagnum* areas only were
196 digitised, for a plot classed as *sphagnum*. These vegetation classes were aggregated according to
197 one of 8 types (Table 1) for ease of classification. In addition, 20 ground control points were
198 identified from Environment Agency Lidar 2m DSM (Environment Agency © 2015) at fixed
199 locations identified using 25cm Aerial imagery (Infoterra, © 2014).

200 **Field data processing: Validation data**

201 Validation points were randomly stratified across the 8 classes in ArcGIS 10.8 (ESRI, 2016),
202 with 10 points within each class. These points were then used to sample the classifications and
203 assess the performance of the random forest classification.

204 **Evaluation and validation**

1
2
3 205 To assess the accuracy of an image classification, a confusion matrix was created which
4
5 206 compared the classification results with the validation data. This identifies the nature of the
6
7 207 classification errors, as well as their quantities. Confusion matrices were produced from the
8
9 208 overlay of the validation areas and the resultant spatial classification. Overall Accuracy (OA)
10
11 209 values were computed from confusion matrices in order to evaluate the accuracy of the produced
12
13 210 land cover maps (Congalton, 1991). User and producer accuracy was also calculated. Producer
14
15 211 accuracy is the fraction of correctly classified pixels with regard to all pixels of that ground truth
16
17 212 class, whereas user accuracy (or reliability) is the fraction of correctly classified pixels with
18
19 213 regard to all pixels classified as this class in the classified image. A kappa statistic (Cohen,
20
21 214 1960), that compares the accuracy of the system to the accuracy of a random system, was
22
23 215 computed against the validation data. Probability estimates derived from the model (the
24
25 216 percentage votes for each pixel) were grouped by class, and the mean taken for each group to
26
27 217 assess the quality of the predictions.
28
29
30
31
32
33

34 218 **Carbon loss Estimation**

35
36
37 219 The area surveyed at Moor House contains a number of erosion features and gullies. One gully is
38
39 220 of considerable size, and an estimate of the net loss of carbon through the peat degradation and
40
41 221 erosion is of interest. From previous studies of the site, a measurement of the eroding gully
42
43 222 carbon density is $69.84 \pm 2.74 \text{ mg C cm}^3$ (Whitfield 2012). The area of the gully was first
44
45 223 covered with a hypothetical surface (assumed flat) at 4 cm spatial resolution, to cover the edges
46
47 224 of the gully, and only where bare peat was exposed. This follows the method of Evans and
48
49 225 Lindsay (2010), who used linear interpolation of the DEM between gully edges defined from the
50
51 226 gully map to create a 'pre-erosion' surface; and then subtracted the contemporary surface from
52
53 227 the pre-erosion surface to create a gully depth map. Using a cut – fill model in QGIS (QGIS
54
55
56
57
58
59
60

228 Development Team, 2017), a hypsometric model of the eroded gully was then created. Using this
229 estimate of volume and the carbon density measurements for the Moor House site allowed an
230 estimate of the carbon loss to be calculated.

231 **Results**

232 The SfM derived imagery yielded a 4 cm resolution orthomosaic (Figure 1). The elevation model
233 obtained from the image processing was used to compute the aspect, slope and topographic index
234 maps shown in Figures 3. The classifications computed by the RF classifier yielded the
235 classification maps and probability estimates in Figures 4 to 7.

236 Confusion matrices were produced to assess the accuracy of the classified image using both data
237 input scenarios (Table 2 and 3). These matrices show the accuracy of the predictions for the
238 external validation areas, which are independent of the training areas used for establishment of
239 the classification models. For scenario 1, using RGB data only, the classification accuracy per
240 class varied between 40 and 100%. The highest classification accuracy in this case was for
241 coniferous woodland, with the lowest being for bare peat. The overall kappa coefficient was 0.66
242 (Table 2). For scenario 2, using RGB and surface topography data, the classification accuracy
243 per class varied between 50 and 100%. The highest classification accuracy was for conifer
244 plantation, and the lowest was for bare peat. The overall kappa coefficient was slightly higher at
245 0.68 (Table 3).

246 Mean probability values for each classification are shown in Figure 7 and ranged from 41%
247 (Saturated bog) to 67% (coniferous woodland). For all classes, the mean classification
248 probability was higher for the RGB plus topography classification.

249 **Carbon loss estimate**

250 The volume of material lost in the formation of the gully, assuming an intact blanket bog
251 formation prior to erosion, was estimated as 6,273 m³. The carbon density for gullies at Moor
252 House is 69.84 ± 2.74 mg C cm³. Therefore the estimated carbon that has been lost from the
253 gully is estimated to be between 420 and 455 tonnes of C.

254 Discussion

255 The results of the image classification using a Random Forest classifier are encouraging, and
256 demonstrate the potential for rapid reconnaissance and monitoring of blanket bog condition (*per*
257 *se*) nationally. Incorporation of surface feature data derived from SfM techniques improved the
258 classification accuracy. The incorporation of surface data improves the classification by defining
259 those areas where water accumulates in the landscape, thereby assisting the classification of the
260 smaller *Sphagnum* bog areas. Incorporation of surface topography improved the predictive
261 accuracy, in part due the presence of specific habitats in dry or wet areas of the blanket bog. For
262 example *Sphagnum* carpet is only ever found in specifically wet channels or funnels at the Moor
263 House site. Conversely, exposed bare peat may only be found on the flat tops or edges of the
264 blanket bog (Bower, 1961), where water accumulates, and hard frost and wind can attack the
265 structure of the peat. The centre of the blanket bog is characterised by a large eroding mass of
266 peat. This is not surprising since peat erosion is associated with high levels of exposure and
267 precipitation (Bragg, 2001; Yeloff et al. 2005). The Random Forest classifier accurately predicted
268 all classes specified in the training data. Interestingly, although the classification accuracy (user
269 accuracy) for bare peat was 50%, saturated bog, water and sphagnum were higher, ranging
270 between 80% and 90%. Saturated bog, water and bare peat habitats are often in very close
271 proximity in the study area, and only by using aerial photography at 4cm resolution could we

272 locate habitat patches at such fine a scale. Future studies could look at how much bare peat exists
273 elsewhere in the study area, in addition to the central exposed peat area.

274 The probability of the classification is slightly higher for all classes when topography is used in
275 addition to the RGB data. This may in part be due to high spatial variability in the surface
276 topography exceeding that encompassed within the training data. Also, the incorporation of more
277 predictor variables in Random Forests may yield greater certainty, as a result of the model
278 structure. The mean probability estimates are acceptable (i.e. generally above the default value of
279 0.5), however it is worth noting that Random Forest classifiers normally give good estimates
280 (Belgiu and Dragut 2016), probably due to the transitional nature of upland habitats. Further
281 studies should explore the effect of sample data collection and survey date on the classification.
282 In some cases an accurate Random Forests model can give poor probability estimates (Yang et
283 al. 2016), so the percentage of correctly classified test data is the most common criterion to
284 evaluate models (Bostrom 2007). Therefore comparison of both scenarios accuracies based on
285 mean probabilities could be misleading.

286 Although the vegetation survey data and the aerial survey were six years apart, the use of site
287 photography taken on the date of the vegetation survey (2010) allowed a comparison of the
288 present situation with the state of the land surface in 2014 to be accomplished, and showed that
289 vegetation composition was not significantly different. We cross referenced photographs from
290 the study site taken at the time of the botanical survey, with 25 cm resolution aerial photography,
291 and our own orthorectified imagery to ensure that the training areas had not changed
292 significantly, thus minimising any uncertainty associated with the classification of training areas.
293 Ideally, vegetation surveys should be undertaken at least during the same year of the aerial
294 survey to reduce this uncertainty.

1
2
3 295 As with all modelling and data collection methodologies there are uncertainties arising from the
4
5 296 various stages of data acquisition, and implicit uncertainties in the modelling, either as a result of
6
7 297 the data or the structure of the modelling framework. The uncertainties in the data may arise
8
9 298 through the temporal mismatch between the date of image acquisition and the land survey, and
10
11 299 this may explain some of the misclassification of water as peat and vice versa.

12
13
14
15 300 The purpose of this study was to investigate the area of blanket peatland under erosion, and
16
17 301 quantify the apparent losses. This was achieved with some success, but also some uncertainty,
18
19 302 since the volume of intact blanket peatland prior to the formation of gully and erosion features
20
21 303 can never be fully known. The true volume of carbon that has been lost cannot be calculated,
22
23 304 since the bog would have gradually lost and simultaneously sequestered carbon through
24
25 305 revegetation and recovery over time. Also, the hypothetical surface used to calculate the volume
26
27 306 could be Estimating a value is, however, useful in providing the conservation scientist with a
28
29 307 value associated with the formation of gully features, and what could potentially be recovered
30
31 308 through habitat restoration.

32
33
34
35
36 309 The methodology, combining ground- and UAV-based survey, and ground control points based
37
38 310 on static objects, is readily transferable to other sites containing different habitats. When
39
40 311 combined with topographic indices, slope and aspect, RGB data can be extremely useful in
41
42 312 remote areas where habitat classification can be difficult due to limited access or data
43
44 313 availability. Although ground control points should normally be located using a high accuracy
45
46 314 GPS unit, such systems were unavailable to the team at the time, and the purpose of this study
47
48 315 was to minimise impact at the site, especially in the upland saturated bog environment. Future
49
50 316 studies could however make use of onboard RTK systems for improved camera location
51
52 317 accuracy, and improved ground control point accuracy for the static locations. While
53
54
55
56
57
58
59
60

1
2
3 318 hyperspectral data from UAVs are still expensive to obtain, the approach provided here can
4
5 319 provide equivalent outputs with a similar level of accuracy. UAVs may therefore fill the gap
6
7 320 between land surveys and satellite imagery. UAVs do have some drawbacks compared to more
8
9 321 traditional sources of remote sensing data. Specifically, UAVs are more limited in their sensor
10
11 322 payload, and therefore the complexity of sensors that they can carry, although this is due to a
12
13 323 combination of cost, ease of use and regulations. UAVs are also more susceptible to high winds
14
15 324 and adverse weather compared to manned aircraft. Wind speeds above 15 knots (35 mph)
16
17 325 typically lead to poor image capture from a UAV. Individual flights cover much smaller areas
18
19 326 compared to manned aircraft and satellites. Therefore more flights are required to cover larger
20
21 327 areas and more time is required to process the imagery produced. Larger areas (multiple km²)
22
23 328 could be captured per flight using fixed wing UAVs, however this approach is limited by visual
24
25 329 flight rule requirements. RGB data from UAV platforms can also fill the gap between field and
26
27 330 satellite imagery, which are either labour intensive or conversely too coarse resolution to
28
29 331 separate distinct habitats within the broad habitats. UAV hyperspectral data are still prohibitively
30
31 332 expensive, so the combination of UAV RGB data with topography data can be useful for upland
32
33 333 habitats in the UK where the access is difficult and availability of satellite imagery is low due to
34
35 334 cloud coverage.
36
37
38
39
40
41
42

43 335 **Conclusions**

44
45 336 There is a greater availability of UAV platforms providing RGB imagery at present, owing in
46
47 337 part to the expense of hyperspectral instruments. This study demonstrates that for large areas of
48
49 338 fairly homogenous and well defined habitats, habitat classifications may be produced in a
50
51 339 relatively cheap and easy way using consumer grade cameras and relatively inexpensive fixed
52
53 340 wing UAV platforms. Remote sensing of upland sites in the UK can be difficult due to cloud
54
55
56
57
58
59
60

1
2
3 341 cover, and therefore UAVs may offer an effective and realistic alternative. Combined with open
4
5 342 source software approaches for image classification, this approach presents new opportunities for
6
7 343 directing, and monitoring the success of peatland conservation schemes. As a specific means of
8
9
10 344 measuring success, carbon loss estimates can be readily generated using the UAV imagery and
11
12 345 SfM techniques described here.

15 346 **Acknowledgments**

17
18 347 We thank the NERC Centre for Ecology and Hydrology for providing the internal funding for
19
20 348 the purposes of this work.
21
22
23
24
25
26
27
28
29
30
31
32
33
34
35
36
37
38
39
40
41
42
43
44
45
46
47
48
49
50
51
52
53
54
55
56
57
58
59
60

350 **References**

- 351 Anderson, K., Bennie, J.J., Milton, E.J., Hughes, P.D.M., Lindsay, R., & Meade, R. (2010)
352 Combining LiDAR and IKONOS Data for Eco-Hydrological Classification of an Ombrotrophic
353 Peatland. *Journal of Environmental Quality*, 39, 260-273
- 354 Anderson, K. and Gaston, K. J. (2013) Lightweight unmanned aerial vehicles will revolutionize
355 spatial ecology. *Frontiers in Ecology and the Environment*, 11: 138–146. doi:10.1890/120150
- 356 Belgiu, M., & Dragut, L. (2016). Random forest in remote sensing: A review of applications and
357 future directions. *Isprs Journal of Photogrammetry and Remote Sensing*, 114, 24-31
- 358 Bostrom, H. (2007) Estimating class probabilities in random forests. In *Machine Learning and*
359 *Applications, 2007. ICMLA 2007. Sixth International Conference on*, pp. 211-216. IEEE, 2007.
- 360 Boyle S.A., Kennedy C.M., Torres J., Colman K, Pérez-Estigarribia P.E., de la Sancha N.U.
361 (2014). High-Resolution Satellite Imagery Is an Important yet Underutilized Resource in
362 Conservation Biology. Peter H-U, ed. *PLoS ONE.*, 9(1):e86908.
363 doi:10.1371/journal.pone.0086908.
- 364 Bower M, (1961). The distribution of erosion in blanket peat bogs in the Pennines. *Transactions*
365 *of the Institute of British Geographers*, 29: 17-30
- 366 Bragg, O M & J H Tallis, (2001) The sensitivity of peat-covered upland landscapes. *Catena*, 42:
367 345-360.
- 368 Breiman L. (2001) Random Forests. *Machine Learning*, 45, 5–32.

- 1
2
3 369 Breiman, L., Friedman, J. H., Olshen, R. A., & Stone, C. J. (1984) Classification and regression
4
5 370 trees. Monterey, CA: Wadsworth & Brooks/Cole Advanced Books & Software. Breiman, L.
6
7 371 1996. Bagging Predictors. *Machine Learning* 24:123-140.
8
9 372
10 373 Cohen, J. (1960) A coefficient of agreement for nominal scales. *Educational and Psychological*
11
12 374 *Measurement* 20, 37-46.
13
14 375
15 376 Congalton RG. (1991) A Review of Assessing the Accuracy of Classifications of Remotely
16
17 377 Sensed Data. *Remote Sensing of Environment* 37: 35-46.
18
19 378
20 379 Dye, M., Mutanga, O., & Ismail, R. (2012) Combining spectral and textural remote sensing
21
22 378 variables using random forests: predicting the age of *Pinus patula* forests in KwaZulu-Natal,
23
24 379 South Africa. *Journal of Spatial Science*, 57, 193-211
25
26 380
27 381 Environmental Systems Research Institute (ESRI) (2010). ArcGIS Release 10. Redlands, CA.
28
29 382
30 383 Evans, C.D., Bonn, A., Holden, J., Reed, M.S., Evans, M.G., Worrall, F., Couwenberg, J., &
31
32 382 Parnell, M. (2014) Relationships between anthropogenic pressures and ecosystem functions in
33
34 383 UK blanket bogs: Linking process understanding to ecosystem service valuation. *Ecosystem*
35
36 384 *Services*, 9, 5-19
37
38 385
39 386 Evans, M. and Lindsay, J. (2010) High resolution quantification of gully erosion in upland
40
41 386 peatlands at the landscape scale. *Earth Surface Processes and Landforms*, 35: 876–886.
42
43 387
44 387 doi:10.1002/esp.1918
45
46 388
47 388 Freeman, C., Evans, C.D., Monteith, D.T., Reynolds, B., & Fenner, N. (2001) Export of organic
48
49 389 carbon from peat soils. *Nature*, 412, 785-785
50
51 390
52 391 Gislason P.O., Benediktsson J.A., & Sveinsson J.R. (2006) Random Forests for land cover
53
54 390 classification. *Pattern Recognition Letters*, 27, 294–300.
55
56 391
57
58
59
60

- 1
2
3 392 Glendell, M., McShane, G., Farrow, L., James, M. R., Quinton, J., Anderson, K., Evans,
4
5 393 M., Benaud, P., Rawlins, B., Morgan, D., Jones, L., Kirkham, M., DeBell, L., Quine, T. A., Lark,
6
7 394 M., Rickson, J., and Brazier, R. E. (2017) Testing the utility of structure-from-motion
8
9 395 photogrammetry reconstructions using small unmanned aerial vehicles and ground photography
10
11 396 to estimate the extent of upland soil erosion. *Earth Surface Processes and Landforms*, 42: 1860–
12
13 397 1871. doi: 10.1002/esp.4142.
14
15
16
17 398 Gorham, E. (1991) Northern peatlands: role in the carbon cycle and probable responses to
18
19 399 climatic warming. *Ecological Applications*, 1: 182-195
20
21
22
23 400 Holden J. (2005) Peatland hydrology and carbon release: why small-scale process matters.
24
25 401 *Philosophical Transactions of the Royal Society a-Mathematical Physical and Engineering*
26
27 402 *Sciences* 363: 2891-2913.
28
29
30
31 403 Horning, N. (2013) Training Guide for Using Random Forests to Classify Satellite Images – v9.
32
33 404 American Museum of Natural History, Center for Biodiversity and Conservation. Available from
34
35 405 <http://biodiversityinformatics.amnh.org/>. [https://doi.org/10.5285/7a7d08e3-48e2-4aad-855b-](https://doi.org/10.5285/7a7d08e3-48e2-4aad-855b-9d6767b9ae9b)
36
37 406 [9d6767b9ae9b](https://doi.org/10.5285/7a7d08e3-48e2-4aad-855b-9d6767b9ae9b)
38
39
40
41 407 Joosten H., Tapio-Biström M.-L. & Tol S. (eds) (2012) Peatlands –guidance for climate change
42
43 408 mitigation through conservation, rehabilitation and sustainable use. 2nd ed. FAO and Wetlands
44
45 409 International, Rome, Italy, 100 pp. ISBN: 978-92-5-107302-5
46
47
48 410 Juel, A., Groom, G.B., Svenning, J.C., & Ejrnaes, R. (2015) Spatial application of Random
49
50 411 Forest models for fine-scale coastal vegetation classification using object based analysis of aerial
51
52 412 orthophoto and DEM data. *International Journal of Applied Earth Observation and*
53
54 413 *Geoinformation*, 42, 106-114
55
56
57
58
59
60

- 1
2
3 414 Liaw and M. Wiener (2002). Classification and Regression by randomForest. R News 2(3), 18--
4
5 415 22.
6
7
8 416 Littlewood, N., Anderson, P., Artz, R., Bragg, O., Lunt, P. and Marrs, R. (2010) Peatland
9
10 417 biodiversity. Report to IUCN UK Peatland Programme, Edinburgh. www.iucn-uk-
11
12 418 peatlandprogramme.org/scientificreviews
13
14
15 419 Magurran, A.E. (1988) Ecological diversity and its measurement. London: Croon Helm Ltd. 179
16
17 420 p.
18
19
20
21 421 Maskell, L.C., Norton, L.R., Smart, S.M., Carey, P.D., Murphy, J., Chamberlain, P.M., Wood,
22
23 422 C.M., Bunce, R.G.H. & Barr, C.J. (2008) *Countryside Survey Technical Report No. 1/07 Field*
24
25 423 *Mapping Handbook*.
26
27 424 http://www.countrysidesurvey.org.uk/sites/default/files/pdfs/reports2007/CS_UK_2007_TR1.pdf
28
29
30
31 425 Mc Morrow, I.M., Cutler, M.E., Evans, M, Alroichdi, A., (2004), hyperspectral indices for
32
33 426 characterising upland peat composition. *International journal of remote sensing*, 25, 313-325.
34
35
36 427 R Core Team (2013). R: A language and environment for statistical computing. R Foundation for
37
38 428 Statistical Computing, Vienna, Austria. URL <http://www.R-project.org/>.
39
40
41 429 QGIS Development Team (2017). QGIS Geographic Information System. Open Source
42
43 430 Geospatial Foundation Project. <http://qgis.osgeo.org>
44
45
46 431 Rodwell, J.S. (ed.) (1995). *British Plant Communities. Volume 4. Aquatic communities, swamps*
47
48 432 *and tall-herb fens*. Cambridge University Press.
49
50
51 433 Rose, R.J., Wood, C.M., Baxendale, C.L., Whitfield, M.G., Ostle, N.J., Driscoll, B., Looker, A.,
52
53 434 Looker, G. (2016). Vegetation survey of Moor House National Nature Reserve 2008-2009.
54
55
56
57
58
59
60

- 1
2
3 435 NERC Environmental Information Data Centre <https://doi.org/10.5285/7a7d08e3-48e2-4aad->
4
5 436 855b-9d6767b9ae9b
6
7
8 437 Smart, S.M. (2000) MAVIS: Modular Analysis of Vegetation Information System.: Centre for
9
10 438 Ecology and Hydrology, Lancaster, UK. Available: <http://www.ceh.ac.uk/services/modular->
11
12 439 analysis-vegetationinformation-system-mavis.
13
14
15 440 Sørensen, R.; Zinko, U.; Seibert, J. (2006) “On the calculation of the topographic wetness index:
16
17 441 evaluation of different methods based on field observations”. *Hydrology and Earth System*
18
19 442 *Sciences*. 10: 101–112.
20
21
22 443 Toth C and Jozkow G. (2016) Remote sensing platforms and sensors: A survey. *Isprs Journal of*
23
24 444 *Photogrammetry and Remote Sensing* 115: 22-36.
25
26
27 445 Whitfield, M.G. Peatland diversity and carbon dynamics, Thesis submitted for the degree of
28
29 446 Doctor of Philosophy, Lancaster University, September 2012.
30
31
32 447 Yang, F., Piao P., and Qifeng, Z. (2016) A preliminary study on class probability estimation for
33
34 448 random forest using kernel density estimators. *Computer Science & Education (ICCSE)*, 2016
35
36 449 11th International Conference on. IEEE, 2016.
37
38
39 450 Yeloff, D.E., Labadz, J.C., Hunt, C.O., Higgitt, D.L., & Foster, I.D.L. (2005) Blanket peat
40
41 451 erosion and sediment yield in an upland reservoir catchment in the southern Pennines, UK. *Earth*
42
43 452 *Surface Processes and Landforms*, 30, 717-733
44
45
46 453 Yu ZC. (2012) Northern peatland carbon stocks and dynamics: a review. *Biogeosciences* 9:4071-
47
48 454 4085.
49
50
51 455
52
53 456
54
55
56
57
58
59
60

457

For Peer Review

- 1
- 2
- 3
- 4
- 5
- 6
- 7
- 8
- 9
- 10
- 11
- 12
- 13
- 14
- 15
- 16
- 17
- 18
- 19
- 20
- 21
- 22
- 23
- 24
- 25
- 26
- 27
- 28
- 29
- 30
- 31
- 32
- 33
- 34
- 35
- 36
- 37
- 38
- 39
- 40
- 41
- 42
- 43
- 44
- 45
- 46
- 47
- 48
- 49
- 50
- 51
- 52
- 53
- 54
- 55
- 56
- 57
- 58
- 59
- 60

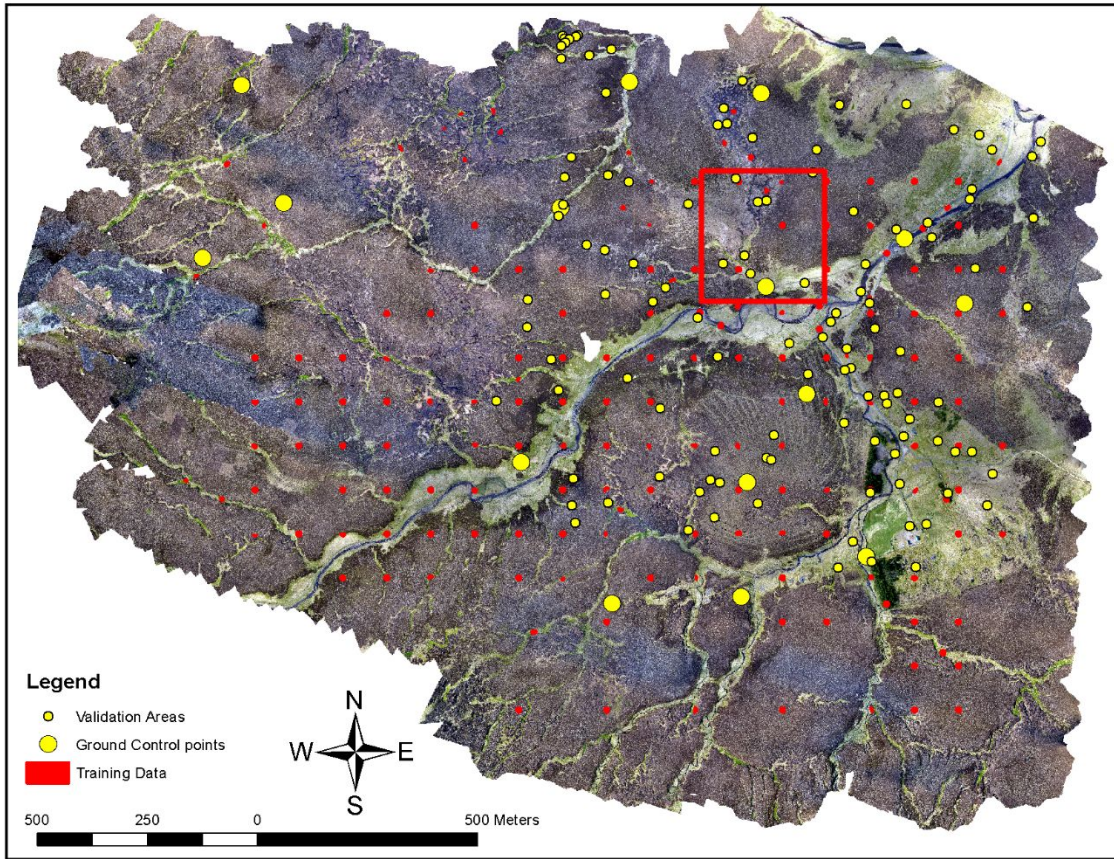


Figure 1 Overview of the Troutbeck study area at Moor House ECN, showing the orthorectified image obtained from 4 UAV flights, ground control points, the model training and validation areas and the focus area (red square).

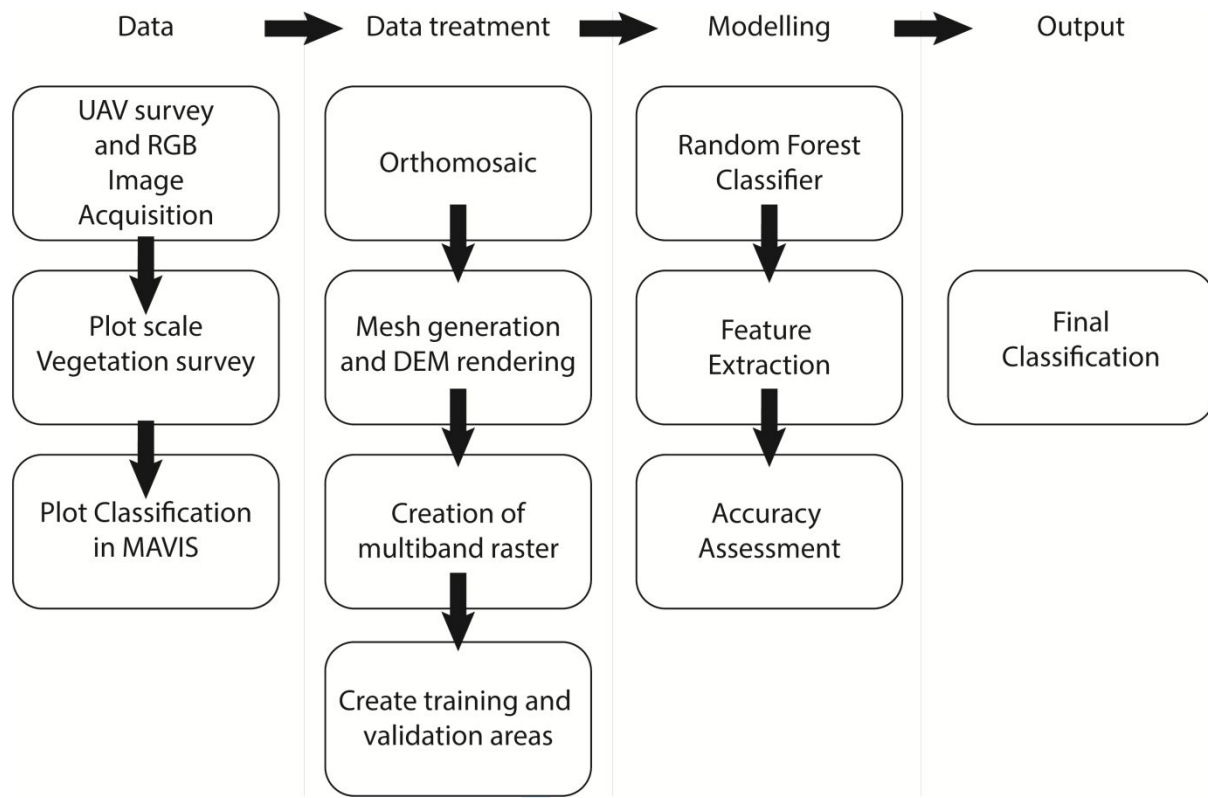


Figure 2 Process flow from image capture to the final habitat classification used in this study.

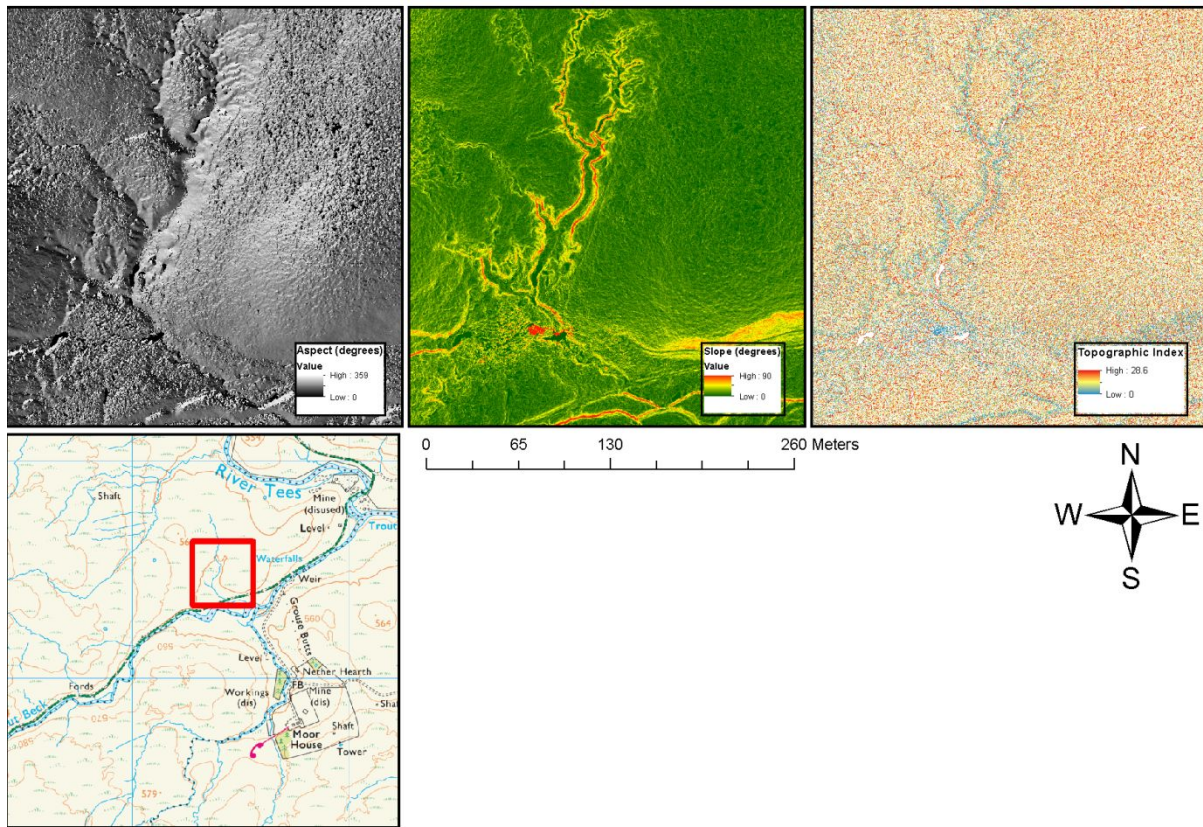
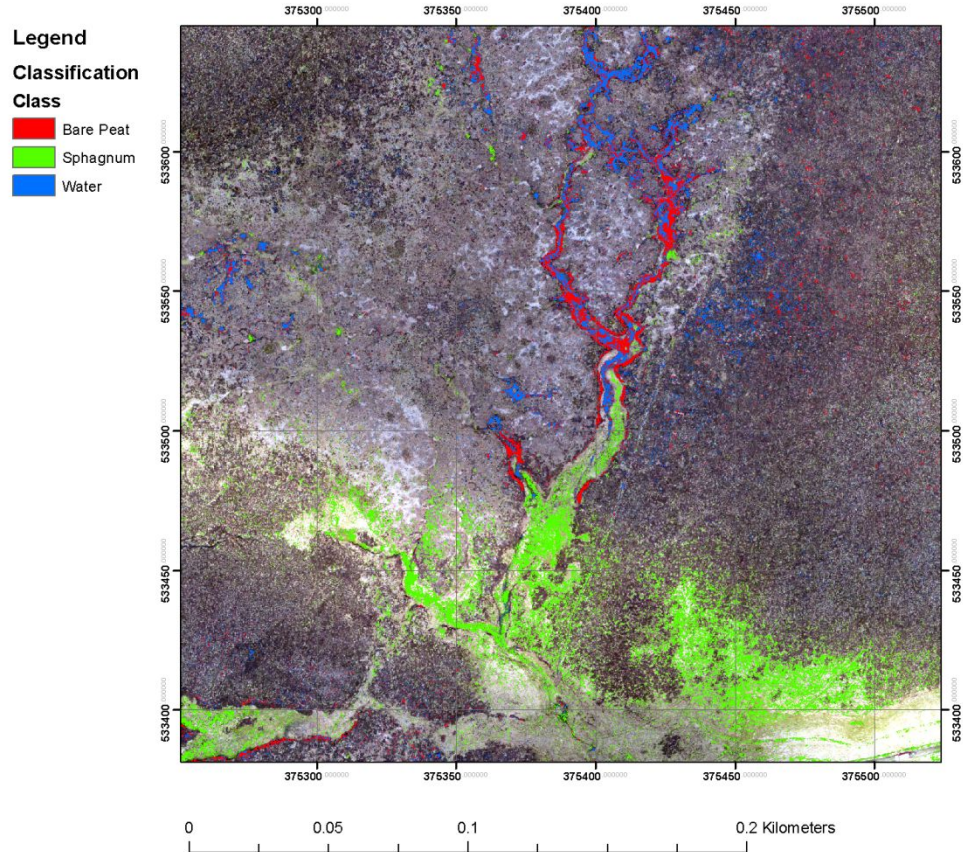


Figure 3 Aspect, slope and topographic index surfaces generated from the surface topography (4 cm spatial resolution). Area of the eroded gully shown, maps extend across the whole Moorhouse study area.



32
33
34
35
36
37
38
39
40
41
42
43
44
45
46
47
48
49
50
51
52
53
54
55
56
57
58
59
60

Figure 6 Map showing the bare peat, water and sphagnum habitats as predicted for Moor House with RGB and topographic information for the focus area.

Legend
RGB Colourspace Model
Class

- Bare Peat
- Conifer plantation
- Gravel/Road
- Northern blanket bog
- Rush/moorland grass/streamside
- Saturated bog
- Sphagnum
- Water

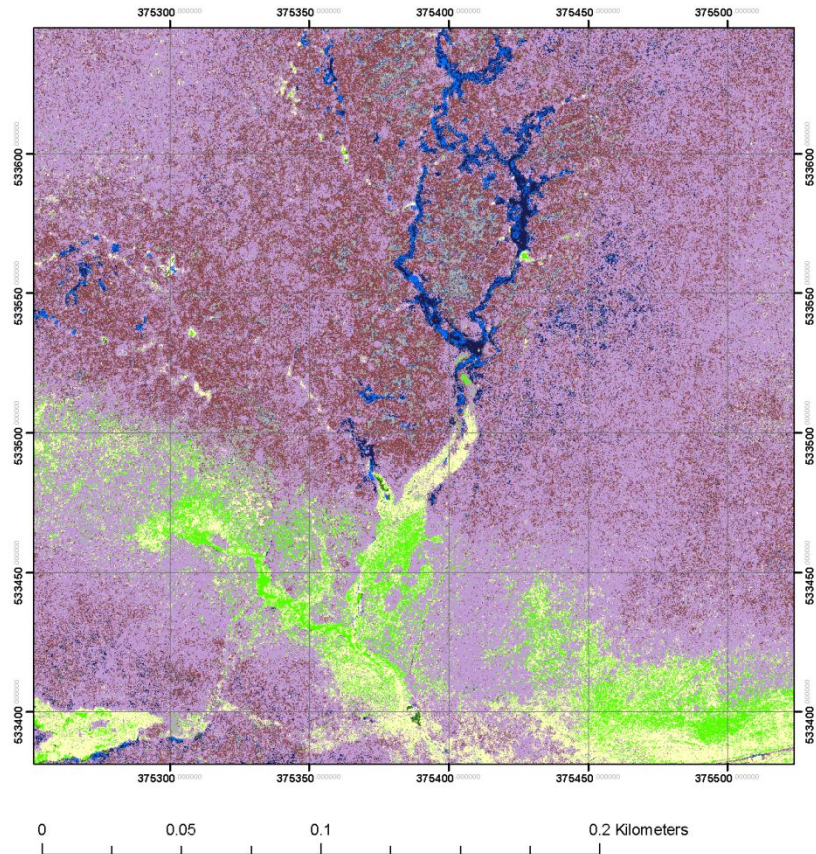


Figure 7 Predicted classes for Moor House using only the RGB data

Review

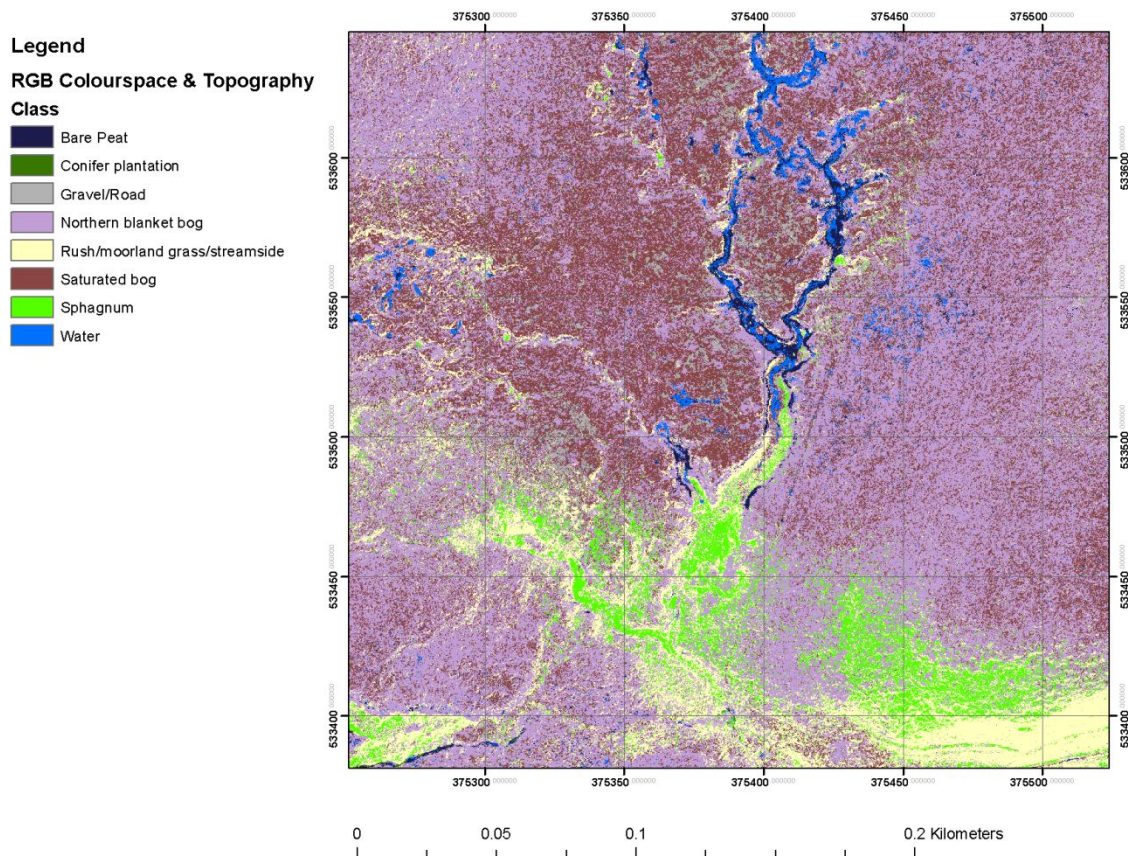


Figure 8 Predicted classes for Moor House using the RGB combined with the topographic information

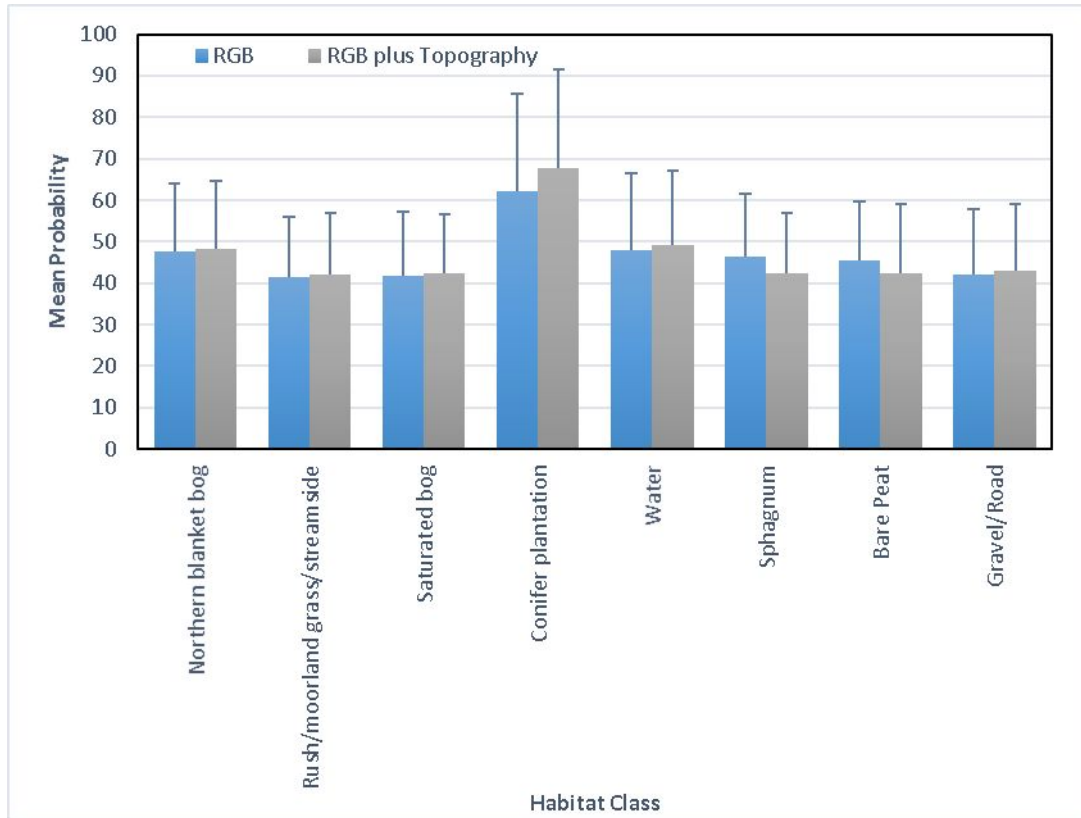


Figure 9 Mean probabilities for each surface summarised for each classification with standard errors.

Table 1 List of aggregated classes based on the Countryside Vegetation System used in this study

CVS Class	Aggregate Class
Northern Blanket Bog	Northern Blanket Bog
Dry heath soil	Bare Peat
Bare Peat	
Young conifer	Conifer plantation
Conifer plantation	
River shingle	Gravel
Streamside/acid grassland	Moorland Grass
Bracken/acid grass	
Moorland grass/bog	
Moorland grass/heath peat	
Marsh/streamside	
Moorland grass/heath soil	
Heath/moorland grass	
Saturated bog	Saturated bog
Sphagnum	Sphagnum
Open Water	Open Water

Table 2 Confusion Matrix for the random forest classification using only the RGB data for Moor House

	Predicted									Total	User accuracy (%)
	Northern blanket bog	Rush/moorland grass/streamside	Saturated bog	Conifer plantation	Water	Sphagnum	Bare Peat	Gravel/Road			
Northern blanket bog	8	0	2	0	0	0	0	0	10	80	
Rush/moorland grass/streamside	0	10	0	0	0	0	0	0	10	0	
Saturated bog	2	1	7	0	0	0	0	0	10	70	
Conifer plantation	0	0	0	9	1	0	0	0	10	90	
Water	0	0	2	0	7	0	0	1	10	70	
Sphagnum	0	1	0	0	0	9	0	0	10	90	
Bare Peat	3	0	1	0	2	0	4	0	10	40	
Gravel/Road	1	0	2	0	0	0	0	7	10	70	
Total	14	12	14	9	10	9	4	8			
Producer accuracy (%)	42	83	50	100	70	100	100	88			
Kappa	0.68										

Table 3 Confusion Matrix for the random forest classification using the RGB data and surface topography for Moor House

		Predicted									Total	User accuracy (%)
		Northern blanket bog	Rush/moorland grass/streamside	Saturated bog	Conifer plantation	Water	Sphagnum	Bare Peat	Gravel/Road			
Actual	Northern blanket bog	9	0	1	0	0	0	0	0	10	90	
	Rush/moorland grass/streamside	1	9	0	0	0	0	0	0	10	90	
	Saturated bog	1	0	8	0	1	0	0	0	10	80	
	Conifer plantation	0	0	0	10	0	0	0	0	10	0	
	Water	1	0	0	1	8	0	0	0	10	80	
	Sphagnum	0	1	0	0	0	9	0	0	10	90	
	Bare Peat	1	1	1	0	2	0	5	0	10	50	
	Gravel/Road	0	2	1	0	0	1	0	6	10	60	
	Total	13	14	11	11	11	10	5	6			
	Producer accuracy (%)	41	64	73	91	73	90	100	100			
Kappa	0.66											

Table 1 Processing parameters used in Agisoft Photoscan for the construction of the orthomosaic and digital surface model

General	Cameras 2207 Aligned cameras 2207 Markers 24 Coordinate system OSGB 1936 / British National Grid (EPSG::27700) Rotation angles Yaw, Pitch, Roll
Point Cloud	Points 440,842 of 638,731 Reprojection error 1.2099 (7.04299 max) Point colors 3 bands, uint8 Key points No Average tie point multiplicity 3.75116
Dense Point Cloud	Points 625,020,795 Point colors 3 bands, uint8
Dense Point Cloud Reconstruction parameters	Quality High Depth filtering Aggressive
Model	Faces 4,925,688 Vertices 2,473,776 Vertex colors 3 bands, uint8 Texture 4,096 x 4,096, 4 bands, uint8
Model Reconstruction parameters	Surface type Height field Source data Dense Interpolation Enabled Quality High Depth filtering Aggressive Face count 5,000,000 Processing time 20 minutes 12 seconds
Model Texturing parameters	Mapping mode Orthophoto Blending mode Mosaic Texture size 4,096 x 4,096 Enable hole filling Yes Enable ghosting filter Yes UV mapping time 1 minutes 37 seconds Blending time 9 hours 46 minutes
DSM	Size 52,504 x 46,139 Coordinate system OSGB 1936 / British National Grid (EPSG::27700)
DSM Reconstruction parameters	Source data Dense cloud Interpolation Enabled Processing time 55 minutes 24 seconds
Orthomosaic	Size 65,494 x 52,584 Coordinate system OSGB 1936 / British National Grid (EPSG::27700) Colors 3 bands, uint8
Orthomosaic Reconstruction parameters	Blending mode Mosaic Surface DEM Enable hole filling Yes Processing time 1 hours 15 minutes

Table 5. Control points RMSE and ground control point (GCP) errors , (X - Easting, Y - Northing, Z – Altitude).

Point type	Count	X error (m)	Y error (m)	Z error (m)	XY error (m)	Total (m)
Control	15	1.75774	0.485608	1.43344	1.82359	2.31953
GCP	Label	X error (m)	Y error (m)	Z error (m)	Total (m)	Image (pix)
	Bridge	-0.469988	-0.100511	-0.728492	0.87275	0.000 (1)
	point 1					
	point 2	-0.499273	0.0301792	0.249121	0.55879	0.000 (1)
	point 3	-0.936561	-0.487554	-1.5222	1.85256	0.002 (4)
	point 4	2.05486	-0.616093	-3.03196	3.71413	0.002 (2)
	point 5					
	point 6	0.0944338	0.510288	0.282165	0.590702	0.000 (1)
	point 7					
	point 8	0.220504	-0.0945066	1.2857	1.30789	0.005 (7)
	point 9	0.261059	-0.448917	2.29679	2.35477	0.003 (3)
	point 10	-0.106125	-0.870693	-1.06144	1.37696	0.005 (3)
	point 11	0.384385	-0.632363	0.320792	0.806562	0.001 (3)
	point 12	0.659767	0.174325	-1.05869	1.25956	0.003 (4)
	point 13					
	point 14					
	point 15					
	point 16	-6.03509	-0.503942	-1.11076	6.15711	0.002 (3)
	point 17					
	point 18					
	point 19	1.41136	-0.343287	1.09074	1.81645	0.003 (3)
	point 20	0.972456	0.651922	1.50597	1.90752	0.003 (3)
	point 21	0.823755	0.0132818	2.07568	2.2332	0.002 (3)
	point 22					
point 23	-0.128602	0.67285	-0.600468	0.910949	0.002 (2)	